Chinese Chemical Letters 33 (2022) 4017–4020

Contents lists available at ScienceDirect

Chinese Chemical Letters

journal homepage: www.elsevier.com/locate/cclet

Surface engineering on segmented copper-iron nanowires arrays

Lingling Du[a], Shizheng Zheng[a], Lijun Zheng[a], Xiaxia Xing[a], Dachi Yang[a,*], Can Xue[b,*]

[a] Department of Electronics, College of Electronic Information and Optical Engineering, Nankai University, Tianjin 300350, China
[b] School of Materials Science and Engineering, Nanyang Technological University, Singapore 639798, Singapore

ARTICLE INFO

Article history:
Received 9 January 2022
Revised 8 February 2022
Accepted 16 February 2022
Available online 19 February 2022

Keywords:
Surface engineering
Segment
Copper-iron nanowires
Wet-chemical etching
Galvanic reaction

ABSTRACT

Surface engineering that could modulate the surface shape to be endowed with the high specific surface ratio, abundant chemical dangling bonds and improved defects exposure is highly desired and needs further exploring. Here, we report a facile strategy of surface engineering on decorating the controllable segmented copper-iron nanowires arrays (Cu-Fe NWs) with their respective hydroxides. Specifically, the pristine segmented Cu-Fe NWs are firstly synthesized *via* sequentially electrodepositing Cu NWs and Fe NWs inside the nanochannels of anode aluminum oxide (AAO) template. Subsequently, the surface and interface of Cu-Fe NWs are wet-chemically etched, in which the metallic Cu and Fe are partially converted into $Cu(OH)_x$ nano-fibrous roots (NFRs) and $FeO(OH)_y$ nanoparticles (NPs), and finally decorate around the respective outer-surface of Cu NWs and Fe NWs segments. As one case of the applications in hydrogen evolution reaction (HER), our surface-modified Cu-Fe NWs exhibit improved catalytic activity compared with Fe NWs.

Nanostructures endowing with a large specific surface area, abundant chemical dangling bonds and defects exposure have been paid increasing attention, which may open up possibilities in optimizing properties of materials and nanodevices [1–4]. Generally, diverse surface engineering has been widely investigated such as the generation of surface defects [5,6], exposure of crystalline facets [7], construction of surface heterostructure [8], and regulation of chemical composition [9], which are expected to understand the structure-property relationships between nanostructures, surface defects, chemical bonds and physical properties. Previous surface engineering ways have been reported such as biomimetic biopolymer coating for decorating functional groups [10], Ar plasma etching and high-temperature treatment for creating vacancies [5,11], and atomic layer deposition for constructing heterostructure [12]. However, such surface engineering ways usually require either sophisticated setups or tedious procedures, little is reported on the facile surface engineering toward the nanostructures such as uniform nanowires-nanowires (NWs-NWs) junctions arrays that simultaneously modulates the surface compositions, shapes and structures.

Recently, the earth-abundant and low-cost metals like iron (Fe), cobalt (Co), nickel (Ni), copper (Cu) and their hybrids have been extensively explored in the energy-related fields [13–15]. Especially, their hydroxides such as $FeO(OH)_y$ are studied considering their intrinsic catalytic activity, environment-friendly nature and the stable and efficient activity in alkaline aqueous solution [16]. However, the poor conductivity and mass-transfer ability of these hydroxides limit the electrocatalytic performance [16]. Previously, CoNi bi-component nanosheets were anchored onto the spaced TiO_2 nanotube arrays for constructing p-n heterojunction [17]. If these hydroxides could be developed *in-situ* upon one-dimensional nanostructures such as nanowires (NWs) or nanotubes, the low conductivity of the hydroxides would be compensated with the fast electronic radial transport in well-controlled nanowires arrays.

In this study, we report a facile surface engineering toward decorating the segmented copper-iron nanowires arrays (Cu-Fe NWs) with the respective hydroxides *via* first anodic aluminum oxide (AAO) template confined electrodeposition and subsequent wet-chemical etching, as illustrated in Fig. 1. Specifically, the Cu-Fe NWs arrays are surface-engineered (SE) around the Cu NWs segments with $Cu(OH)_x$ nano-fibrous roots (NFRs), and the Fe NWs ones with $FeO(OH)_y$ nanoparticles (NPs) in Fig. 2a, respectively.

In our surface engineering, the AAO template confined synthesis and the resultant segmented-NWs junctions with the geometrical parameters are controllable and tunable at will. Specifically, the segmented-NWs junctions are confined in the channels of AAO template, and their geometrical parameters such as diameter and length can be tuned by the geometrical ones of the AAO template [18]. Also, the segmented NWs inside the nanochannels can be modulated by the sequence and duration in the AAO

* Corresponding authors.
E-mail addresses: yangdachi@nankai.edu.cn (D. Yang), cxue@ntu.edu.sg (C. Xue).

https://doi.org/10.1016/j.cclet.2022.02.038
1001-8417/

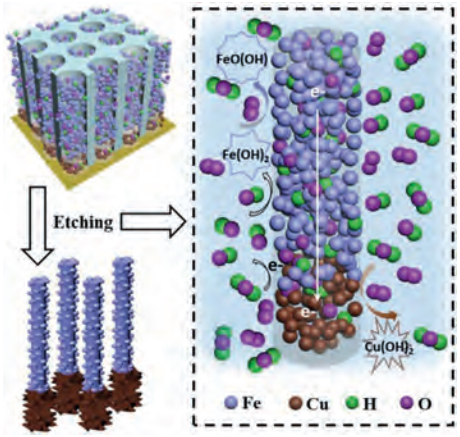

Fig. 1. Schematic illustration of the surface engineering towards SE Cu-Fe NWs.

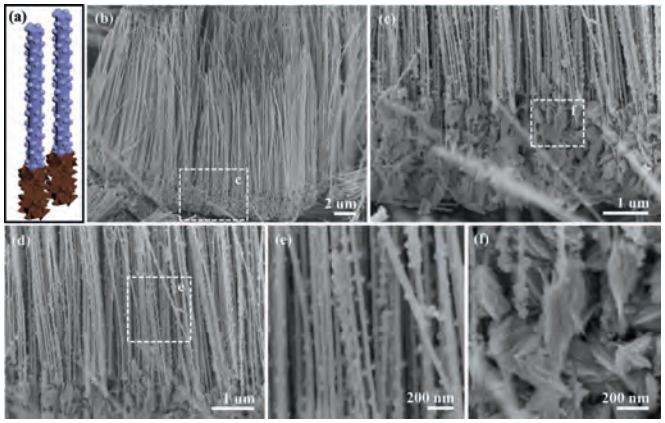

Fig. 2. Micro-structural characterization of SE Cu-Fe NWs. (a) Schematic nanostructure. (b-d) SEM images under low magnifications. Magnified SEM images of (e) Fe NWs and (f) Cu NWs segments.

template-confined electrodeposition [18,19]. Hence, Cu-Fe NWs junctions arrays are taken as examples and the experimental details are provided in Supporting information. In Figs. 2b-d, the scanning electron microscopy (SEM) images show the representative SE Cu-Fe NWs arrays. Notably, the distinct shapes are observed from the top-segments of Fe NWs with NPs (Fig. 2e) and the bottom-ones of Cu NWs with NFRs (Fig. 2f). To verify the chemical composition, a line-scanning energy-dispersive X-ray spectroscopy (EDS, Fig. 3) was taken along the longitudinal axis of the representative SM Cu-Fe NWs arrays, and revealed that the Cu and Fe elements exhibited well-defined distribution at the lower and upper segments of these NWs, respectively.

Sequentially, we further characterized the representative Fe NWs and Cu NWs segments on SE Cu-Fe NWs with transmission electron microscopy (TEM). In case of Fe NW segment (Figs. 4a and b), the NPs located on the trunk of Fe NW segment are around 100 nm in diameter. Further, the lattice spaces of ~0.4262 nm and ~0.2656 nm are found on the NPs in the high-resolution TEM (HR-TEM) image (Fig. 4c), which correspond to the (110) and (130) planes of FeO(OH), respectively. Meanwhile, these lattice spaces consistent with the Fe (110) planes and FeO(OH) (130) planes are observed on the trunk (Figs. S1a-c in Supporting information), suggesting that metallic Fe partially converts into $FeO(OH)_y$ NPs on the surface of Fe NWs segments during the chemical etching. By contrast, the NFRs are decorated around the "trunk" along Cu NWs segment (Figs. 4d and e), which may provide large surface ratio [20]. In Fig. 4f, the lattice spaces of ~0.2622 nm correspond to the (002) planes of $Cu(OH)_2$ in the fibrous roots, and the ones corre-

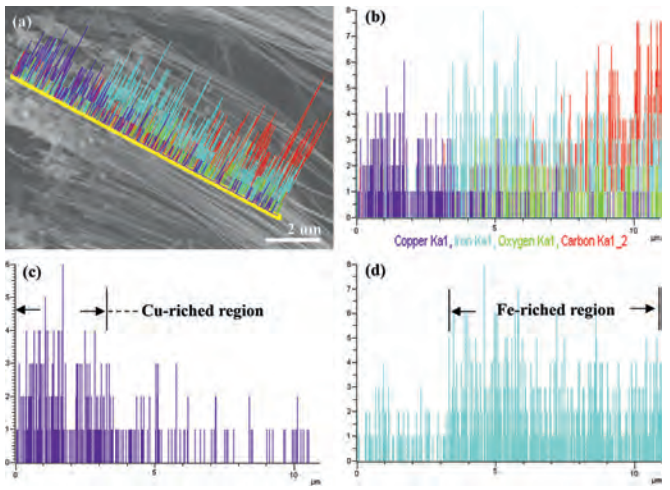

Fig. 3. EDS analysis of SE Cu-Fe NWs. (a) The analyzed region taken in the SEM image. (b) The mixed elemental distribution. The separated elemental distribution of (c) Cu and (d) Fe elements.

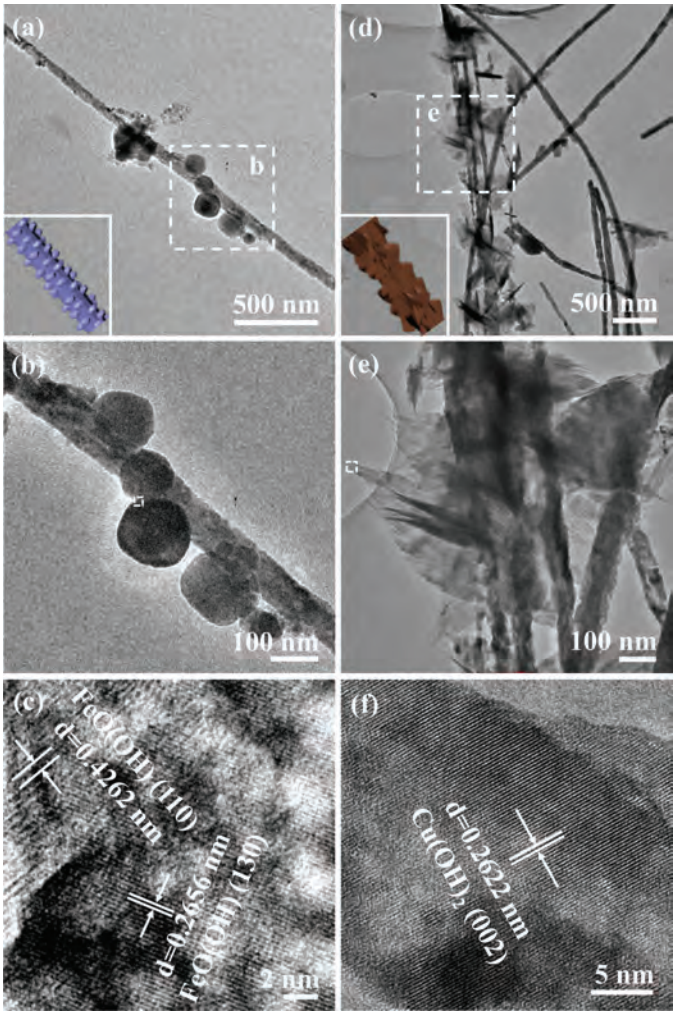

Fig. 4. TEM images of SE Cu-Fe NWs. (a, b) TEM images of Fe NWs segment. (c) HR-TEM image taken from the dashed rectangle in (b). (d, e) TEM images of Cu NWs segment. (f) HR-TEM image taken from the dashed rectangle in (e).

spond to the Cu (111) and the $Cu(OH)_2$ (002) planes in the trunk (Figs. S1d-f in Supporting information). Accordingly, partial metallic Cu on the surface of Cu NWs is converted into $Cu(OH)_x$ *via* the wet-chemical modification.

To get insight into the surface engineering toward SE Cu-Fe NWs, we electrodeposited only Cu NWs or Fe NWs inside the AAO templates, and Figs. S2 and S3 (Supporting information) show the SEM images of the Cu NWs and the Fe NWs after dissolving the templates, respectively. We can see that both the Cu NWs and the Fe NWs present cylindrical shape with rough surface that might be etched in NaOH solution. By contrast, the SE Cu-Fe NWs exhibit much rougher surface being modified by their hydroxides (Fig. 2), which might provide a larger surface area for boosting HER catalytic reaction. To testify the role of additional etching solution, we dropped $FeCl_2$ solution into the Cu NWs dispersion and kept overnight, the similar fibrous root-shaped networks were found covered around the Cu NWs (Fig. S4 in Supporting information). As revealed that the Fe species play a crucial role in the surface modification, and the modification reactions (Eqs. 1–3) are proposed below.

$$4Fe^{2+} + O_2 + 2H_2O = 4Fe^{3+} + 4OH^- \quad (1)$$

$$2Fe^{3+} + Cu = 2Fe^{2+} + Cu^{2+} \quad (2)$$

$$Cu^{2+} + 2OH^- = Cu(OH)_2 \quad (3)$$

Due to the O_2 from the air, the Fe^{2+} ions in H_2O react with the O_2 for Fe^{3+}. In this case, more OH^- is generated, which promotes more metallic Cu being etched and more $Cu(OH)_x$ NFRs being formed.

Similarly, during the dissolution and etching of AAO template in 4 mol/L NaOH solution, a surface modification occurs simultaneously on the Cu-Fe NWs. In this case, the Cu NWs segment, Fe NWs segment and NaOH solution would constitute a "galvanic corrosion" reaction, similar to the previous reports [21,22]. As shown in Fig. 1, the oxidation-reduction reactions (Eqs. 4 and 5) occur as follows.

$$O_2 + 2H_2O + 4e^- = 4OH^- \quad (4)$$

$$Fe - 2e^- = Fe^{2+} \quad (5)$$

In above reactions, the electronegativity difference between metallic Fe and Cu induces the etching of Fe NWs segment. Subsequently, the similar wet-chemical reactions (Eqs. 1–3) further take place on the surface of Cu-Fe NWs. Meanwhile, the nucleation and growth of iron hydroxides on Fe NWs segment are achieved *via* below reaction 6.

$$4Fe^{2+} + O_2 + 8OH^- = 4FeO(OH) + 2H_2O \quad (6)$$

Actually, the Cu NWs segment and Fe NWs segment play the crucial roles in the surface modification. As a result, the heterostructure construction has been achieved on the surface of SE Cu-Fe NWs, in which the $FeO(OH)_y$ NPs are anchored the Fe NWs segment and $Cu(OH)_x$ NFRs are decorated on Cu NWs segment, respectively. The $FeO(OH)_y$ and $Cu(OH)_x$ are self-assembled around the surface of Fe NWs segment and Cu NWs one, respectively, which might be caused by the high surface energy and the lattice mismatch between the Cu species and Fe one [23,24]. In such heterostructure, the $FeO(OH)_y$ NPs and $Cu(OH)_x$ NFRs enhance the specific surface area and the metallic core inside Cu-Fe NWs facilitates the electron transfer [25]. With the characterization of X-ray diffraction (XRD) of the SE Cu-Fe NWs (Fig. S5 in Supporting information), one can see that these diffractive peaks match the body-centered cubic crystalline Fe (PDF#06-0609), face-centered cubic crystalline Cu (PDF#04-0836), orthorhombic-phase FeO(OH) (PDF#29-0713) and $Cu(OH)_2$ (PDF#13-0420), respectively. The result together with the TEM characterizations confirm the compositions of SE Cu-Fe NWs, in accordance with above proposed wet-chemical modification.

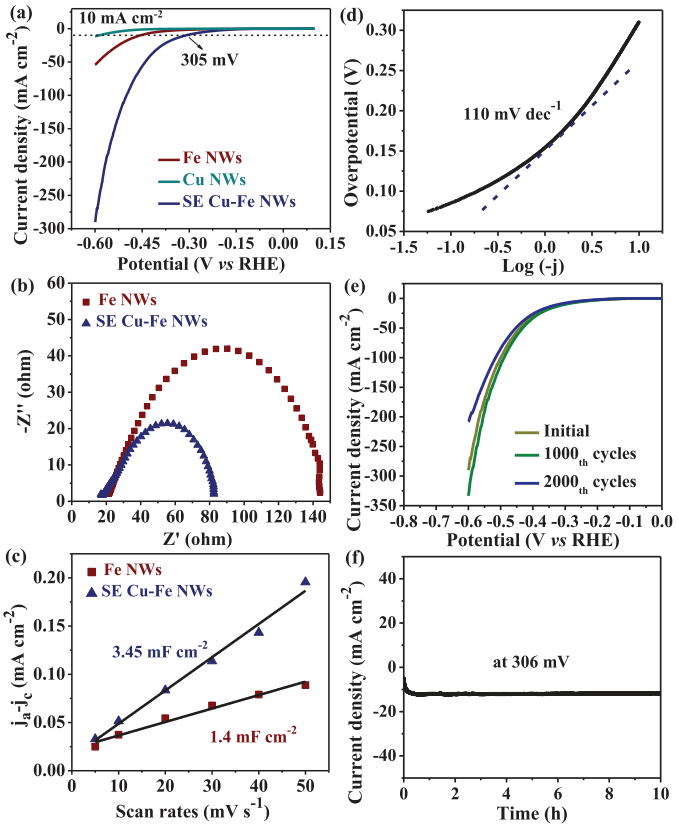

Fig. 5. The HER evaluations in 1 mol/L KOH. (a) LSV curves. (b) Nyquist Plots. (c) The capacitive current densities as a function of scan rate. (d) Tafel plot. (e) LSV curves before and after 1000 and 2000 CV cycles. (f) Time-dependent current density.

Moreover, the chemical states of elements on the surface of SE Cu-Fe NWs were analyzed by X-ray photoelectron spectroscopy (XPS). In case of O 1s spectrum, we can see that the binding energy of O 1s in SE Cu-Fe NWs shifts more positively about 0.24 eV compared to that of Fe NWs (Fig. S6a in Supporting information). Further, the O 1s spectrum in SE Cu-Fe NWs can be deconvoluted into two oxygen species (Fig. S6b in Supporting information), in which the lower binding energy is assigned to oxygen bonding with metal (O-M), and the higher one assigned to the hydroxyls and chemisorbed oxygen [26]. These results reveal the peak of O 1s corresponding to surface hydroxyls (O-H) is dominant in SE Cu-Fe NWs. Meanwhile, both Cu 2p and Fe 2p spectra were well-fitted with two spin orbit doublets as well as shakeup satellites, characteristic of their mixed oxides and hydroxides (Figs. S6c and d in Supporting information). These results indicate that the wet-chemical modification promotes the generation of hydroxides upon the surface of Cu-Fe NWs. As is reported [27], the hydroxides promote water dissociation and the concomitant interaction to boost the formation of intermediates for adsorbing hydrogen atoms.

FeOOH-based materials have been investigated and hold great potential in the fields of energy storage and conversion devices [28,29]. Accordingly, as one example of application, the SE Cu-Fe NWs were evaluated as catalysts toward hydrogen evolution reaction (HER) in 1 mol/L KOH. Fig. 5a shows the linear sweep voltammetry (LSV) curves of Fe NWs, Cu NWs and SE Cu-Fe NWs. Clearly,

the SE Cu-Fe NWs exhibit the smallest overpotential of 305 mV at 10 mA/cm, showing higher catalytic activity than Fe NWs and Cu NWs. Further, the electrochemical impedance spectroscopy (EIS) in Fig. 5b shows that the semicircle diameter of the SE Cu-Fe NWs is much smaller than that of Fe NWs, suggesting faster charge transfer kinetics. To understand the HER catalytic activity, the cyclic voltammetry (CV) curves tests of the SE Cu-Fe NWs and Fe NWs were carried out in Fig. S7 (Supporting information) for estimating the electrochemical active surface area (ECSA). In Fig. 5c, the double-layer capacitance (C_{dl}) of 3.45 mF/cm^2 for the SE Cu-Fe NWs is larger than the C_{dl} of 1.4 mF/cm^2 for Fe NWs, indicating that the SE Cu-Fe NWs expose more active surface via surface engineering. As a result, the SE Cu-Fe NWs possess superior HER activity with a Tafel slope of 110 mV/dec (Fig. 5d). It is noted that the activity of SE Cu-Fe NWs is comparable to those of the reported Cu or Fe compounds-based HER catalysts (Table S1 in Supporting information) [30–35]. In addition, both the negligible overpotential shift of LSV over 2000 CV cycles (Fig. 5e) and the chronoamperometric test for 10 hours (Fig. 5f) demonstrate the SE Cu-Fe NWs with excellent HER stability. Taken together, the improved HER performance of SE Cu-Fe NWs is ascribed to the synergistic effect of the surface modification of $Cu(OH)_x$ NFRs and $FeO(OH)_y$ NPs that exposes large catalytic area, and their heterostructure of Cu NWs/$Cu(OH)_x$ NFRs and Fe NWs / $FeO(OH)_y$ NPs that facilitates the electron transfer.

In summary, the segmented Cu-Fe NWs modified with their hydroxides have been achieved via firstly sequential electrodeposition of the Cu and Fe NWs within the nanochannels of AAO templates and the subsequent wet-chemical etching. By utilizing the "galvanic corrosion" reaction constituted by Cu, Fe and NaOH solution, the metallic Cu and Fe on the surface of segmented Cu-Fe NWs in the wet-chemical etching are partially converted into $Cu(OH)_x$ NFRs and $FeO(OH)_y$ NPs, which are decorated around the surface of Cu NWs and Fe NWs segment, respectively. Interestingly, the junctions between segments of Fe NWs decorating $FeO(OH)_y$ NPs and ones of Cu NWs decorating $Cu(OH)_x$ NFRs have been achieved. In this study, our surface engineering strategy towards the uniform NW-NW segmented junctions with modified metallic hydroxide, may be extended to other bimetallic junctions arrays that could be obtained *via* template-confined synthesis, and are then proposed for further decorating defects and chemical bonds, and improving surface ratio.

Declaration of competing interest

The authors declare that they have no known competing financial interests or personal relationships that could have appeared to influence the work reported in this paper.

Acknowledgments

This work was financially supported by the National Natural Science Foundation of China (No. 21473093), and the Fundamental Research Funds for the Central Universities, Nankai University (No. 63191745). C. Xue thanks the support from the Ministry of Education, Singapore, under AcRF-Tier2 (No. MOE2018-T2-1-017) and AcRF-Tier1 (Nos. MOE2019-T1-002-012, RG102/19).

Supplementary materials

Supplementary material associated with this article can be found, in the online version, at doi:10.1016/j.cclet.2022.02.038.

References

[1] P. Chen, Y. Tong, C. Wu, Y. Xie, Acc. Chem. Res. 51 (2018) 2857–2866.
[2] B. Yao, J. Zhang, X. Fan, et al., Small 15 (2019) e1803746.
[3] J.O. Zoppe, N.C. Ataman, P. Mocny, et al., Chem. Rev. 117 (2017) 1105–1318.
[4] W. Luo, X. Chen, Y. Xia, et al., Adv. Energy Mater. 7 (2017) 1701083.
[5] J. Xiong, J. Di, J. Xia, et al., Adv. Funct. Mater. 28 (2018) 1801983.
[6] D. Liu, D. Chen, N. Li, et al., Angew. Chem. Int. Ed. 59 (2020) 4519–4524.
[7] X. Han, G. He, Y. He, et al., Adv. Energy Mater. 8 (2017) 1702222.
[8] M. Liu, Z. Zhao, X. Duan, Y. Huang, Adv. Mater. 31 (2019) e1802234.
[9] K. Mori, T. Sano, H. Kobayashi, H. Yamashita, J. Am. Chem. Soc. 140 (2018) 8902–8909.
[10] R. Liu, J. Zhao, Q. Han, et al., Adv. Mater. 30 (2018) e1802851.
[11] Y. Wang, Y. Zhang, Z. Liu, et al., Angew. Chem. Int. Ed. 56 (2017) 5867–5871.
[12] J. Xie, J. Zhao, Y. Liu, et al., Nano Res. 10 (2017) 3754–3764.
[13] L. Yu, H. Zhou, J. Sun, et al., Energy Environ. Sci. 10 (2017) 1820–1827.
[14] Q. Sun, M. Zhou, Y. Shen, et al., J. Catal. 373 (2019) 180–189.
[15] J. Mohammed-Ibrahim, X. Sun, J. Energy Chem. 34 (2019) 111–160.
[16] H. Li, Q. Zhou, F. Liu, et al., Appl. Catal. B: Environ. 255 (2019) 117755.
[17] Z. Gao, Z. Li, C. Zhao, et al., Catal. Today (2022) doi:10.1016/j.cattod.2022.01.011.
[18] D. Yang, G. Meng, S. Zhang, et al., Chem. Commun. (2007) 1733–1735.
[19] D. Yang, G. Meng, C. Zhu, X. Zhu, Chem. Commun. (2009) 7110–7112.
[20] T. Liu, X. Ma, D. Liu, et al., ACS Catal. 7 (2016) 98–102.
[21] L. Du, L. Zheng, H. Wei, et al., ACS Appl. Nano Mater. 2 (2019) 1178–1184.
[22] L. Zheng, D. Yang, R. Chang, et al., Nanoscale 9 (2017) 8918–8924.
[23] C. Priester, G. Grenet, Phys. Rev. B 61 (2000) 16029–16032.
[24] P. Mohammadi, L.P. Liu, P. Sharma, R.V. Kukta, J. Mech. Phys. Solids 61 (2013) 325–340.
[25] D. Deng, K.S. Novoselov, Q. Fu, et al., Nat. Nanotechnol. 11 (2016) 218–230.
[26] M. Li, L. Tao, X. Xiao, et al., ChemCatChem 10 (2018) 4119–4125.
[27] Q. Liu, E. Wang, G. Sun, Chin. J. Catal. 41 (2020) 574–591.
[28] D. Friebel, M.W. Louie, M. Bajdich, et al., J. Am. Chem. Soc. 137 (2015) 1305–1313.
[29] J.Q. Xie, Y.Q. Ji, J.H. Kang, et al., Energy Environ. Sci. 12 (2019) 194–205.
[30] J. Hu, Y. Liu, ChemistrySelect 6 (2021) 4129–4134.
[31] F. Rosalbino, G. Scavino, M. Actis Grande, J. Electroanal. Chem. 694 (2013) 114–121.
[32] X. Du, G. Ma, Y. Wang, et al., Dalton Trans. 50 (2021) 14001–14008.
[33] K. Wu, Y. Meng, X. Li, et al., Intermetallics 125 (2020) 106820.
[34] Z. Zhang, B. He, L. Chen, et al., ACS Appl. Mater. Inter. 10 (2018) 38032–38041.
[35] X. Xu, Y. Chen, W. Zhou, et al., Adv. Mater. 28 (2016) 6442–6448.